Nanosize Iron Oxide for CO Oxidation

Zhihua Wu, Martin Fransson and Bing Zhou

Headwaters Technology Innovations LLC
1501 New York Avenue
Lawrenceville, NJ 08648
E-mail: zwu@headwaters.com

ABSTRACT

Transition metal oxides are desirable alternatives to precious metals based catalysts for CO oxidation since they are less costly. Several nanosize iron oxides were prepared by using Headwaters Technology Innovation (HTI) NxCat® colloidal chemistry nanotechnology. These catalysts were applied on CO oxidation and showed better performance than bulk iron oxide, and comparable performance to catalyst with 100 ppm Pd loading. The particle size of iron oxide veries with calcination temperature. When anneal temperature is below 300°C, the particle size of iron oxide is less than 10 nm based on TEM and XRD characterizations and is mainly existed as Fe_3O_4. At SV=600,000 h^{-1}, the advantage of nanosize iron oxide (3-5 nm) in onset activity is over 100°C compared to bulk iron oxide.

Keywords: nanosize iron oxide, carbon monoxide, oxidation

1 INTRODUCTION

The formation of CO has been of concern in many industrial processes. Transition metal oxides are desirable alternatives to the precious metals based CO catalysts for many of these applications since they are less costly. Nanosize transition metal oxides could potentially provide significantly improved catalytic performance over micron size materials, due to their high surface area and more densely populated surface unsaturated sites.

2 EXPERIMENTAL METHODS

2.1 Test System

Catalyst screening tests were conducted in a tubular flow system. 100 mg of catalyst samples were dusted onto quartz wool, which was then placed into a quartz flow tube and sandwiched with additional glass wool. The flow tube was then placed in a temperature-controlled tube furnace. The sample temperature was monitored by a K-type thermocouple inserted into the dusted quartz wool, and another thermocouple was placed in the middle of the furnace, outside the flow tube for monitoring the furnace temperature. Temperature data was recorded by computer. Heating rate was 12°C/min

Reactant gases were introduced as a pre-mixed gas feed containing 2.94% of carbon monoxide, 21.00% of oxygen, and helium as the carrier gas. Gas flow was controlled at 1000 ml/min by a digital mass flow controller. Samples of effluent gas were collected in a 125 ml cylinder every 2 minutes, and analyzed using a gas chromatograph (HP-6890).

2.2 Powder Catalyst Preparation

Catalysts were prepared using HNI's proprietary NxCat™ dispersion technology[1]. This method is based on the synthesis of a liquid dispersion containing nanoparticles of the active catalytic metal(s), where nanoparticle formation is controlled and adjusted by the use of selected chemical agents, referred to as nanodispersion agents or control agents.

2.3 X-ray Diffraction

XRD data was collected with a Siemens D5000 diffractometer using Cu radiation at 40KV/30mA over the range of 10° to 80° with a step size of 0.05° and a count time of 20 seconds per step.

2.4 Electron Microscopy

Samples of the powdered catalyst and precursor solutions were characterized by using high resolution transmission microscopy (TEM), scanning transmission electron microscopy (STEM), and energy dispersive X-ray analysis (EDXA). The microscope used was a JEOL 2010F TEM/STEM state-of-the-art field emission transmission electron microscope with capabilities ranging from nanobeam and convergent beam diffraction to high resolution phase contrast, analytical and energy filtered imaging.

3 RESULTS AND DISCUSSION

3.1 Effect of Palladium Content

The use of palladium as a promoter was evaluated, and initially, palladium-only catalysts were synthesized in order to determine the baseline performance of the precious metal component. Three samples were synthesized using $CaCO_3$ as the support while varying the palladium loading from 1-100 ppm. As shown in Figure 1, there were very large differences in catalytic activity over this loading range. The catalyst with only 1 ppm palladium showed very low overall activity, while the high loading of 100 ppm resulted in a catalyst with a sharp onset of activity just above 250ºC, reaching nearly full conversion at 300 ºC. The performance of the 10 ppm loading was intermediate.

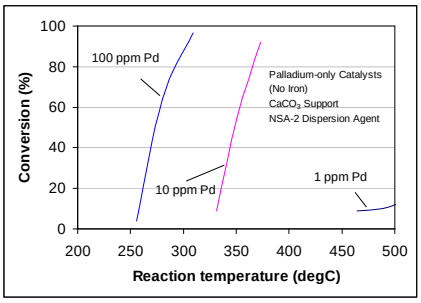

Fig 1: Activity of Pd/CaCO3 catalyst

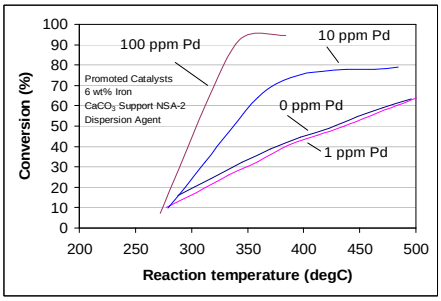

Fig 2: Effect of Pd promotion of 6%Fe/CaCO3

These results indicated a strong catalytic effect of palladium, and that effective palladium loadings were in the 10 to 100 ppm range. Catalysts were prepared including both iron and palladium in order to determine their combined catalytic effect, and to identify any synergistic effects. Tests were carried out using a 6% Fe loading on $CaCO_3$ with palladium loadings from 0-100 ppm. The results in Figure 2 showed a clear transition in catalyst behavior with varying palladium loadings. In the absence of palladium, the onset of catalytic activity for the 6% Fe catalyst on $CaCO_3$ was ~ 250ºC, followed by a gradual increase in conversion, reaching 60% at 500ºC. With the addition of 1 ppm palladium there was no detectable change in the performance as compared to the Fe-only catalyst, confirming the low 1 ppm Pd activity observed in Figure 1. At a 10 ppm loading the effect of the palladium in the 6% Fe catalyst became evident. While the onset temperature for CO conversion was unaffected, the slope of the conversion-temperature curve was significantly steeper, with the conversion reaching 80% at 400ºC. At the 100 ppm Pd level the effect was even more pronounced, with nearly full conversion attained at 350ºC, but interestingly the onset temperature was again unaffected by the Pd addition.

When comparing the data presented in Figures 1 and 2, there is a significant difference in the behavior of Pd-containing catalysts with and without iron present.

3.2 Effect of Activation Temperature

To explore the high-temperature activation treatment effects on the catalyst performance, Fe-only catalysts were prepared and activated at different temperatures. Samples were activated at 50°C, 80°C, 300°C, 500°C, and named as A50, A80, A300, A500, respectively. And one sample was activated using a heated IR-lamp. Figure 3 show the differences in activity between the studied catalysts. When comparing Curve 1 and 2 in Figure 3, it is clear that the activity of the catalyst activated at 50°C was very low, and that the temperature was not sufficient to induce activation. The sample treated at 300°C exhibited the highest activity among these samples. The trend between 50-300°C was that a higher activation temperature lead to a higher activity, but this did not hold true for the catalyst activated at 500°C.

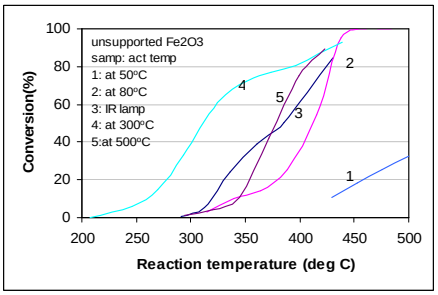

Fig 3: Effect of activation temperature

3.3 Thermogravimetric(TG) and Differential Thermal Analysis(DTA)

Sample catalyst A80 was annealed at 80 °C before the TG/DTS analysis was carried out by heating the sample at rate of 3 °C/minute in a 20 ml/minute air flow. The thermogravimetric curve is a measure of how much of weight the sample loses during the oxidation. After a small initial decline there was a substantial weight loss between ~175-300 °C, after which the sample weight stabilized.

In the temperature interval in which the weight loss occurred, the thermal differential curve indicated that an

exothermic reaction was taking place by the peak in the 200-300°C regime. This was most likely due to residual organic material being burnt off, and from 300-360°C the curve flattens out since there was no organic material left. Just after 360°C an endothermic phase transition process took place exhibiting the characteristic no increase in temperature as more heat was supplied until the entire phase transition had taken place.

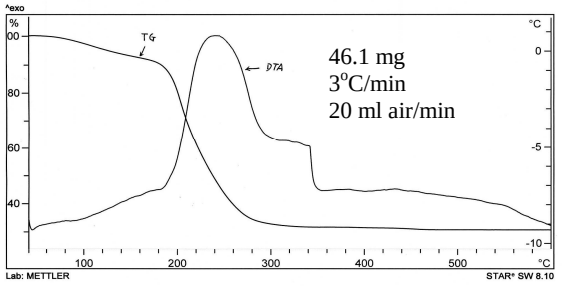

Fig 4: TG and DTA pattern analysis of A80

3.4 X-ray Diffraction

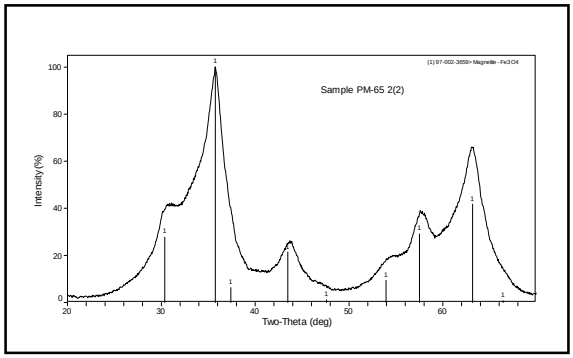

Fig 5: XRD pattern of sample A300

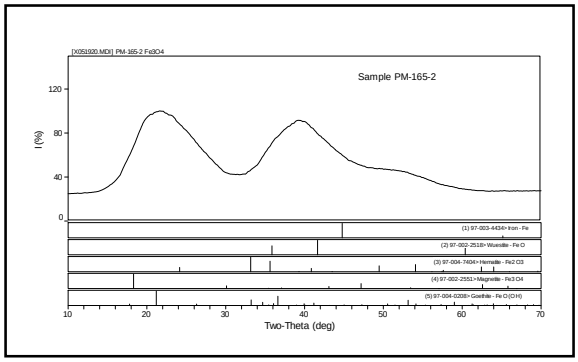

Fig 6: XRD pattern of sample A80

Figure 5 shows the experimental pattern for the sample A300 along with the stick pattern for the identified phase. The material appeared to be phase pure Fe_3O_4 (Magnetite). Due to the very significant amount of broadening, it was difficult to see if another phase was present. Under normal circumstances, X-ray diffraction is described as a 1% method, where second phases as low as 1% can be detected. However, when the peaks are as broad as they were in this sample, the detection limit is closer to 10%. This effect could be seen by noting that the weaker peaks for Magnetite were almost invisible in the pattern.

The particle size in this sample was very small as evidenced by the extremely broad peaks. In earlier samples the half-widths varied from 0.5° to 0.9°. In the present case, the half-widths were much larger (~3.1° FWHM) indicating a much smaller particle size. For this analysis, no single peak could be used since there was too much overlap of the tails from the neighboring peaks. Instead, a whole pattern fitting procedure was done, which indicated an average particle size of 20Å.

Note that the lower limit on particle size detection was much smaller than the normal limit of about 100Å. In the present case that limit can be pushed since the Fe_3O_4 was essentially phase pure and there was no interference from peaks of other phases. Also, Magnetite is cubic and has relatively few diffraction peaks. Thus, they are well separated and the broadening of individual lines could be seen. If there had been many more diffraction peaks, then they would have merged into a continuous, almost featureless background.

As can be seen from Figure 6, the XRD pattern for A80 exhibited three very broad peaks centered at 21.7°, 39.6°, and 51.9°. There are two ways to interpret this pattern. One is that the material was non-crystalline with a high degree of short-range order. Alternatively, the material may have been crystalline with extremely fine particle size in the 20Å range. In order to rule in favor of a crystalline phase, a pattern with peaks in the correct positions must be found. This was attempted with the stick patterns at the bottom of Figure 6. Shown are the patterns for Fe, FeO, Fe_2O_3, Fe_3O_4, and FeO(OH), but none of these matched the experimental pattern. Certainly, the Fe_3O_4 was a poor match. The closest match was FeO(OH), but this was also not a high quality match. Therefore, it seemed unlikely that the material had any of these crystal forms.

Since a crystalline structure could not be found to match the experimental pattern, it was concluded that the material was likely to be a glassy structure with significant short-range order. When an amorphous material has a weak ordering, only a single hump in the XRD pattern is present. But as the ordering improves, a second hump, and then a third hump appear. Finally, as the material progresses to a fully crystalline phase, the humps sharpen into a series of distinct peaks at roughly the same location as the amorphous humps. Therefore, the number of humps is a rough indication of the extent of short-range and long-range order. In the present case, the appearance of three humps

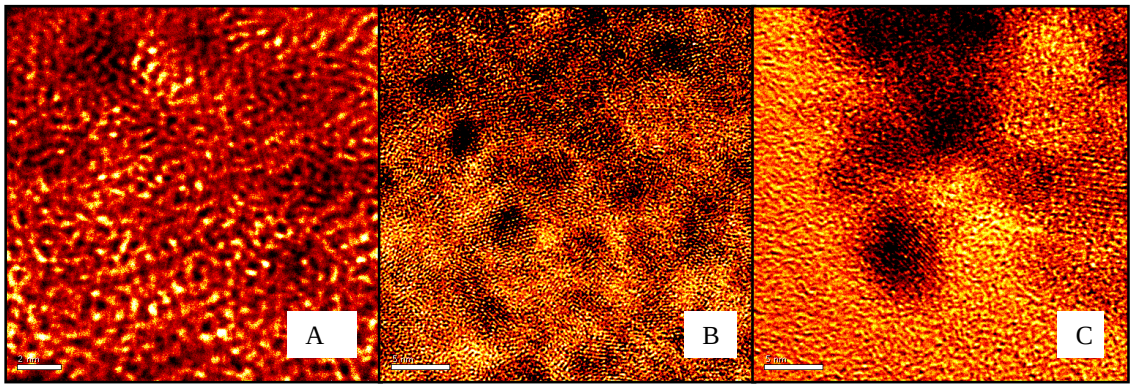

Fig 7: TEM patterns: (A) precursor, (B) A80 and (C) A300

indicated that the material was on the verge of becoming crystalline, but that it was still on the amorphous side of the transformation.

3.5 Electron Microscopy

The precursor was prepared using NxCat™ dispersion technology into a colloid solution. A drop of the solution was placed onto a TEM microscope grid and allowed to evaporate. At higher magnification the particles were determined to be ≤ 3nm. The particles were at least partially crystalline since individual lattice domains could be seen under the right conditions. Three different measurements yielded an average lattice spacing of 0.282nm.

The iron oxide sample A80 was activated at 80°C. It was dark grey/black in color and tiny reflections from the coarse grains could be seen with the naked eye. The crystallites were visible at 5 nm resolution and it was possible to discern the spherical crystallites in an organic matrix. The average size of the crystallites were about 3-4 nm and some lattice could also be observed. The average lattice spacing in six locations was determined to be 0.260 nm.

In appearance A300 large aggregates (>100nm) were observed, which were in turn made up of smaller crystallites approximately in the 3-10 nm size range. The lattice of the crystallites was evident, but the boundaries of the particles were somewhat obscured, perhaps by the presence of an organic phase. Contrary to the other samples for which a similar organic phase was observed, A300 was activated by annealing at the higher temperature of 300°C. In measuring the lattice plane distance, two different values were obtained, 0.256 nm and 0.307 nm. This could be due to that different phases of iron oxide were present in the sample.

The sample activated by annealing at 80°C was semi-amorphous with very small particles generating some short range order, it was not possible to assign an iron oxide phase using XRD. This was confirmed by TEM where 3-5 nm sized crystallites were observed in an organic precursor matrix. The TGA data verifies the presence of an organic phase at temperatures < 160°C, after which it started to burn off. The onset and 40% conversion temperatures was ~300°C and the calculated lattice plane spacings was 0.260 nm.

The sample activated at 300°C in air consisted almost exclusively of Fe_3O_4 and had crystallite sizes in the 3-7 nm range which, was confirmed by both electron microscopy and XRD with good agreement. The sample had a lattice spacings of 0.307 nm. This could be explained by a phase change around its annealing temperature of 360°C, as was observed in the TGA analysis of A80. Common denominators are the dominating Fe_3O_4 phase, lattice spacings of ~ 0.30nm, and less organic precursor remnants from annealing at temperatures ≥ 300°C.

3.6 Summary

The best performing catalyst was activated by annealing in air at ~300°C to reduce the organic precursor content. Annealing at this temperature also favored the preferred iron oxide phase which was Fe_3O_4 (Magnetite), with a crystallite size ≤ 5nm. The best observed catalytic performance was for catalyst sample A300, which showed and onset temperature for CO oxidation at 190°C with a 40% conversion at 265°C.

REFERENCES

[1] Bing Zhou, Sukesh Pasasher, Michael Rueter and Zhihua Wu, US Patent Application 20060174902.